Chem. Soc. Rev., 1986, **15**, 335—371

Recent Developments in the Characterization of Oxide Sols using Small Angle Neutron Scattering Techniques

By J. D. F. Ramsay
CHEMISTRY DIVISION, AERE, HARWELL, OXFORDSHIRE

1 Introduction

Some of the first systematic investigations of colloids were made with oxide sols by Freundich in the early part of this century.[1,2] His pioneering research was extensive and included theoretical and experimental studies of colloid stability, the rheological and light scattering behaviour of colloids under shear, thixotropy, and the flow birefringence of ordered structures of particles.[3–10] These investigations were performed with dilute oxide sols, which included iron oxide,[4,5] vanadium pentoxide,[8] silica,[7] and alumina,[3] and helped lay the foundations for the classic theory of lyophobic colloid stability, subsequently developed by Derjaguin, Landau, Verwey, and Overbeek (DLVO).[11]

Following the work of Freundlich interest in this field of colloid science declined over a period of approximately thirty years, but has been revived more recently by Matijevic whose group has prepared and studied the properties of several monodispersed dilute oxide sols.[12–17] Important technological landmarks were however reached in the fifties and sixties firstly by the commercial development of concentrated silica sols by Iler and others at DuPont[18,19] and secondly with the production of ceramic oxide reactor fuels using sol/gel processes, stimulated by the nuclear industry. Interest in the latter area led to the development, mainly at the

[1] H. Freundlich, 'Kapillarchemie', 1st Edn., Leipzig, 1909.
[2] See *e.g.* 'Colloid Science', ed. H. R. Kruyt, Elsevier, Amsterdam, London, 1952.
[3] H. Freundlich and N. Ishizaka, *Trans. Faraday Soc.*, 1913, **9**, 66.
[4] H. Freundlich and G. Landau, *Kolloid Z.*, 1928, **44**, 198.
[5] H. Freundlich and A. Rosenthal, *Kolloid Z.*, 1925, **37**, 129.
[6] H. Freundlich and F. Juliusberger, *Trans. Faraday Soc.*, 1935, **31**, 920.
[7] D. W. Gillings and H. Freundlich, *Trans. Faraday Soc.*, 1938, **34**, 649.
[8] H. Freundlich, *Z. Electrochem.*, 1916, **22**, 27.
[9] H. Freundlich, *Trans. Faraday Soc.*, 1927, **23**, 614.
[10] H. Freundlich, *Ber. Deutsch. Chem. Ges.*, 1928, **61**, 2219.
[11] E. W. J. Verwey and J. Th. G. Overbeek, 'Theory of Stability of Lyphobic Colloids', Elsevier, Amsterdam, 1948.
[12] R. Demchak and E. Matijevic, *J. Colloid Interface Sci.*, 1969, **31**, 257.
[13] R. Brace and E. Matijevic, *J. Inorg. Nucl. Chem.*, 1973, **35**, 3691.
[14] E. Matijevic, *J. Colloid Interface Sci.*, 1977, **58**, 374.
[15] E. Matijevic, *Acc. Chem. Res.*, 1981, **14**, 22.
[16] H. Tamura and E. Matijevic, *J. Colloid Interface Sci.*, 1982, **90**, 100.
[17] E. Matijevic, *Ann. Rev. Mater. Sci.*, 1985, **15**, 483.
[18] M. F. Bechtold and O. E. Snyder, U.S. Patent 2574902 (1951).
[19] R. K. Iler, 'The Chemistry of Silica', Wiley and Sons, N.Y. 1979, p. 312.

Oak Ridge Laboratory in the U.S.A.[20–23] and Harwell in the U.K.,[24–26] of various processes for the production of concentrated sols of a range of different oxides, whose properties were only understood rather empirically at that stage. Since that period there has been a renewed interest in sol/gel processes in non-nuclear applications, which has increased markedly in the last few years by demands for new specialized ceramic materials.[27–29]

During the past decade there has also been a rapid advance in the understanding of concentrated dispersions of colloidal particles.[30] This progress has mainly been achieved by applying statistical mechanical theories of liquids to the colloid state.[31,32] and by the introduction of new experimental techniques, such as small angle neutron scattering[33] (SANS) and dynamic light scattering.[34] Another factor has been the availability of model colloid systems with well defined properties. Aqueous dispersions of polymer latex particles, which being spherical and uniform in size (monodispersed) are ideal systems, have consequently been studied extensively[35,36] using SANS, although several investigations have been made with concentrated oxide sols.[37–39] In the latter, the particles are in most cases smaller ($\lesssim$ 50 nm), more polydispersed, and have less well defined surface characteristics. Nevertheless a knowledge of structure and the nature of the interactions in oxide dispersions is important in numerous technological applications and has a wider significance for a better understanding of colloid stability and the properties of oxide/water interfaces.

In this short review the general properties of oxide colloids and the ways in which they are formed will be described briefly with an emphasis on concentrated sols. Secondly an outline will be given of the methods which have been used to study

[20] D. E. Ferguson, O. C. Dean, D. A. Douglas, Proc. 3rd Int. Conf. Peaceful Uses At. Energy, Geneva, 1964, (U.N., New York, 1965), Vol. 10, pp. 307—312.
[21] J. G. Moore, Oak Ridge National Laboratory Report (ORNL-4095), 1967.
[22] C. J. Hardy, S. R. Buxton, and M. H. Lloyd, (ORNL-4000), 1967.
[23] M. H. Lloyd and O. K. Tallent, *Nucl. Technol.*, 1973, **18**, 205.
[24] C. J. Hardy, in 'Sol–Gel Processes for Ceramic Nuclear Fuels', Proc. of a Panel, Vienna, 1968, (IAEA, Vienna, 1968), p. 33.
[25] J. M. Fletcher and C. J. Hardy, *Chem. Ind.*, 1968, 48.
[26] R. M. Dell, Proc. 7th Int. Symp. Reactivity of Solids, ed. J. S. Anderson, Chapman and Hall, London, 1972, p. 553.
[27] R. L. Nelson, J. D. F. Ramsay, J. L. Woodhead, J. A. Cairns, and J. A. A. Crossley, *Thin Solid Films*, 1981, **81**, 329.
[28] J. L. Woodhead and D. L. Segal, *Chem. Br.*, 1984, **20**, 310.
[29] J. J. Zelinski and D. R. Uhlman, *J. Phys. Chem. Solids*, 1984, **45**, 1069.
[30] See *e.g.* 'Concentrated Colloidal Dispersions', *Faraday Discuss. Chem. Soc.*, 1983, **76**.
[31] E. Dickinson, in 'Colloid Science', ed. D. H. Everett (Specialist Periodical Reports), The Royal Society of Chemistry, London, 1983, Vol. 4, p. 150.
[32] W. van Megen and I. Snook, *Adv. Colloid Interface Sci.*, 1984, **21**, 119.
[33] R. H. Ottewill, in 'Colloidal Dispersions', ed. J. W. Goodwin, Royal Society of Chemistry, London, 1982, p. 143.
[34] P. N. Pusey and R. J. A. Tough, *Faraday Discuss. Chem. Soc.*, 1983, **76**, 123.
[35] K. Alexander, D. J. Cebula, J. W. Goodwin, R. H. Ottewill, and A. Parentich, *Colloids Surf.*, 1983, **7**, 233.
[36] D. J. Cebula, J. W. Goodwin, G. C. Jeffrey, R. H. Ottewill, A. Parentich, and R. A. Richardson, *Faraday Discuss. Chem. Soc.*, 1983, **71**, 37.
[37] J. D. F. Ramsay and B. O. Booth, *J. Chem. Soc., Faraday Trans. 1*, 1983, **79**, 173.
[38] J. D. F. Ramsay, R. G. Avery, and L. Benest, *Faraday Discuss. Chem. Soc.*, 1983, **76**, 53.
[39] J. Penfold and J. D. F. Ramsay, *J. Chem. Soc., Faraday Trans. 1*, 1985, **81**, 117.

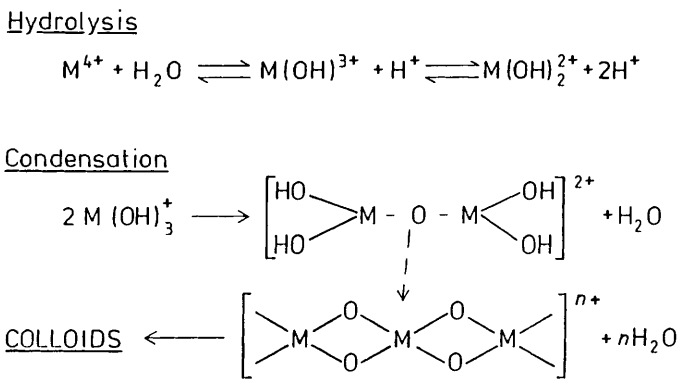

Figure 1 *Hydrolysis and polymerization of polyvalent metal ions in aqueous solution*

these systems, with particular reference to recent applications of the small angle neutron scattering technique.

2 The Formation and Characteristics of Oxide Sols

A. Cation Hydrolysis.—A schematic mechanism in which hydrous oxide or hydroxide colloids are formed from an aqueous solution of metal cations is illustrated in Figure 1. This step-wise process involves the hydrolysis of a solvated aquo-ion followed by condensation to give a polynuclear ion. Such a sequence of hydrolytic and condensation reactions leads, under conditions of oversaturation of the metal hydroxide, to the formation of colloidal hydroxy-polymers which can eventually form hydroxide or hydrous oxide precipitates. This tendency for cation hydrolysis, involving the coordination of –OH ligands (which act as electron pair donors) increases with the acidity, or charge density of the metal ion. Consequently ions of small ionic radius and high charge are extensively hydrolysed in solution, as is illustrated by silicic acid, $Si(OH)_4$, which can exist as a monomer in aqueous solutions of high pH.[19] The tendency for hydrolysis can furthermore be generalized for a wide range of cations as is demonstrated by the dependence of the first hydrolysis constant K_1, on the ratio of the charge to the M–O distance (z/d) shown in Figure 2. The tendency for cation hydrolysis is also paralleled by the ease of polynuclear ion formation. Thus most trivalent and quadrivalent ions form polynuclear species, whereas the process only occurs with the smallest of the divalent ions, Be^{2+}.[40] Such polynuclear species are formed by oversaturating a salt solution with respect to the solid hydroxide or hydrous oxide, by adding a base for example.

This process can be illustrated by the behaviour of aqueous solutions of Fe^{3+} for which the following equilibrium constants have been reported.[41]

[40] G. Schwarzenback and H. Wenger, *Helv. Chim. Acta*, 1969, **52**, 644.
[41] W. Stumm and J. J. Morgan, 'Aquatic Chemistry', Wiley Interscience, New York, 1981.

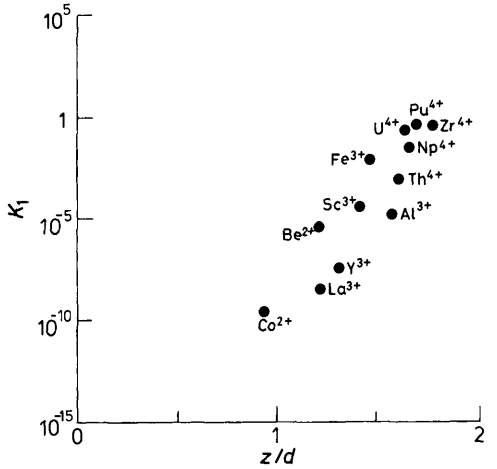

Figure 2 *Dependence of the first hydrolysis constant, K_1, on the ratio of the charge, z, to* M–O *distance, d, for different cations*

$$Fe^{3+} + H_2O \rightleftharpoons FeOH^{2+} + H^+ \qquad \log K_1 = -3.05 \qquad (1)$$

$$Fe^{3+} + 2H_2O \rightleftharpoons Fe(OH)_2^+ + 2H^+ \qquad \log K_2 = -6.31 \qquad (2)$$

$$2Fe^{3+} + 2H_2O \rightleftharpoons Fe_2(OH)_2^{4+} + 2H^+ \qquad \log K_{22} = -2.91 \qquad (3)$$

$$Fe(OH)_3(s) + 3H^+ \rightleftharpoons Fe^{3+} + 3H_2O \qquad \log K_{s0} = 3.96 \qquad (4)$$

$$Fe(OH)_3(s) + H_2O \rightleftharpoons Fe(OH)_4^- + H^+ \qquad \log K_{s4} = -18.7 \qquad (5)$$

Using the representative equilibrium constants, which have been determined by a variety of techniques including potentiometric measurements and spectrophotometry, it is possible to construct distribution diagrams for the different species, as depicted in Figure 3. In the hatched areas shown the solutions become oversaturated with respect to $Fe(OH)_3(s)$ ($K_s = 10^{-38}$) and in consequence polynuclear hydrolysis species will form as intermediates in the formation of $Fe(OH)_3(s)$ which occurs in this range of relatively low pH. If neutralized completely, solutions of Fe^{3+} ions will rapidly precipitate $Fe(OH)_3$ which may age to form crystalline β-FeOOH. Furthermore, in alkaline solution (pH $\gtrsim$10) the formation of ferrate ions, $Fe(OH)_4^-$, becomes increasingly important.

Although there is extensive evidence for the existence of small polynuclear ions[42] containing a few metal atoms [*e.g.* $Be_3(OH)_3^{3+}$, $Zr_4(OH)_8^{8+}$, $Th_2(OH)_2^{6+}$] the structure and stoicheiometry of larger thermodynamically stable species still remain obscure. This is due partly to a lack of suitable techniques for characterizing such small macromolecules, and to the time-dependent and

[42] C. F. Baes and R. E. Messmer, 'The Hydrolysis of Cations', Wiley Interscience, New York, 1976.

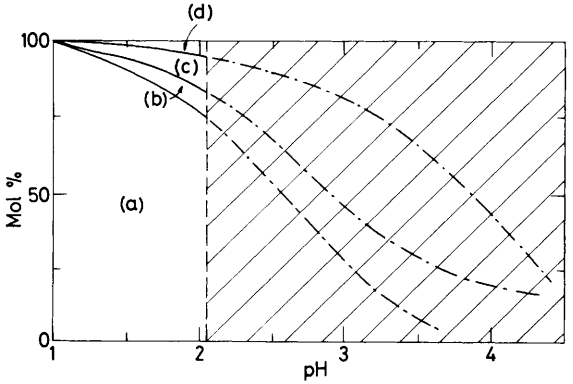

Figure 3 *Distribution diagram for* Fe^{III} *species in aqueous solution at a total* Fe^{III} *concentration of* 10^{-2} mol dm^{-3} *as a function of pH. (a), (b), (c), and (d) correspond to proportions of* Fe^{3+}, $FeOH^{2+}$, $Fe_2(OH)_2^{4+}$, *and* $Fe(OH)_2^+$ *respectively. Broken line corresponds to saturation limit with respect to* $Fe(OH)_3(s)$. – • – *depicts proportion of metastable species in hatched zone where polynuclear hydrolysis species will form as intermediates before the eventual precipitation of the hydroxide occurs*

heterogeneous nature of many aqueous systems which may contain a variety of species simultaneously. Hydrolysed aluminium salt solutions have been among the systems most widely studied[43–46] and here there is evidence for both $Al_8(OH)_{20}^{4+}$ and $Al_{13}O_4(OH)_{24}^{7+}$ species in solution. Novel information which can be obtained from light scattering and incoherent neutron scattering measurements on reasonably well defined and relatively concentrated (> 0.1 mol dm^{-3}) polynuclear ion solutions containing Zr^{IV} and Al^{III} have also recently been reported.[47,48]

B. Sol Formation.—A vast number of specialized procedures are described in the Patent literature for the preparation of oxide sols. The basis of these is sometimes obscure but, in general, colloid formation is achieved either by controlled nucleation and growth processes in solution or by the peptization of powders or precipitates of metal oxides and hydroxides. The mechanism of the first process is frequently based on the controlled growth from a seed nucleus, first described by

[43] J. W. Akitt, N. N. Greenwood, B. L. Khandelwal, and G. D. Lester, *J. Chem. Soc., Dalton Trans.*, 1972, 604.
[44] J. K. Ruff and S. Y. Tyree, *J. Am. Chem. Soc.*, 1958, **80**, 1523.
[45] D. N. Waters and M. S. Henty, *J. Chem. Soc., Dalton Trans.*, 1977, 1977.
[46] J. Y. Bottero, D. Tchoubar, J. M. Cases, and F. Flessinger, *J. Phys. Chem.*, 1982, **86**, 3367.
[47] J. D. F. Ramsay and R. M. Richardson, in 'Water at Interfaces', ed. C. Poinsignon and P. Timmins, Institut Laue Langevin Workshop, 1981, Report 81 TO 55S, p. 105.
[48] J. D. F. Ramsay, in 'Water and Aqueous Solutions', ed. G. W. Neilson and J. E. Enderby, Proc. Colston Symp., Adam Hilger, Bristol, 1986, p. 207.

Zsigmondy[49] and later refined and developed by La Mer[50–52] for the preparation of monodispersed colloids. This is illustrated simply in Figure 4 by the behaviour which occurs when a reaction proceeds and produces a partially soluble product, such as an oxide or hydroxide for example, having a solute concentration, C_p. In this process C_p will rise, passing the saturation concentration, C_s, until the critical supersaturation or nucleation concentration is reached, C_n. At this point nuclei will form, and proceed to grow at a rate determined by the diffusion of neighbouring solute species, which are consumed. This growth process will continue until the solute concentration falls to C_s. To obtain a monodispersed system, nucleation should occur in a short time interval or burst; growth must then proceed by the slow production of solute species which have adequate time to diffuse to the seed nuclei, thus avoiding a reoccurrence of supersaturation and further nucleation. These principles have been applied to numerous systems, particularly by Matijevic[15] and others, to produce sols such as chromium hydroxide,[12] aluminium hydroxide,[13] and silica.[18,53]

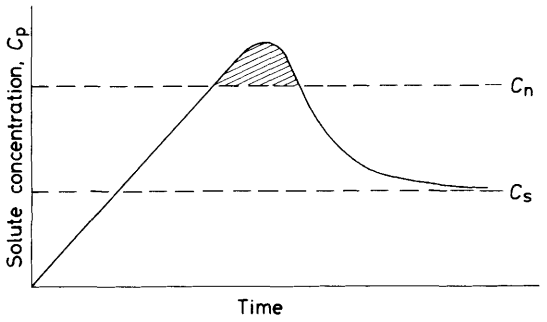

Figure 4 *Diagram illustrating the formation of a colloidal dispersion by controlled nucleation and growth. Initially the solute concentration C_p rises passing the saturation limit, C_s, and continues until the critical nucleation concentration is reached, C_n, at which precipitation occurs in the hatched zone. Further controlled growth of these nuclei results in a decrease in C_p as depicted*

The stability and fate of particles so formed depends on their surface properties and the nature of the aqueous medium. Two distinct situations can arise depending on the interparticle interactions. In the first, where there is strong interparticle repulsion, discrete particles remain as a stable colloidal dispersion. This situation occurs where the particles have a high surface charge and the concentration of electrolyte in the solution is low. For monovalent counterions this is typically $< 10^{-3}$ mol dm^{-3}, although for silica stability may still be maintained up to $\sim 10^{-1}$ mol dm^{-3}. Where these conditions are not fulfilled the particles will tend to

[49] R. Zsigmondy and E. Hückel, *Z. Physik. Chem.*, 1925, **116**, 291.
[50] V. K. La Mer and M. D. Barnes, *J. Colloid Sci.*, 1946, **1**, 71.
[51] D. Sinclair and V. K. La Mer, *Chem. Rev.*, 1949, **44**, 245.
[52] V. K. La Mer and R. H. Dinegar, *J. Am. Chem. Soc.*, 1950, **72**, 4847.
[53] W. Stöber, A. Fink, and E. Bohn, *J. Colloid Interface Sci.*, 1968, **26**, 62.

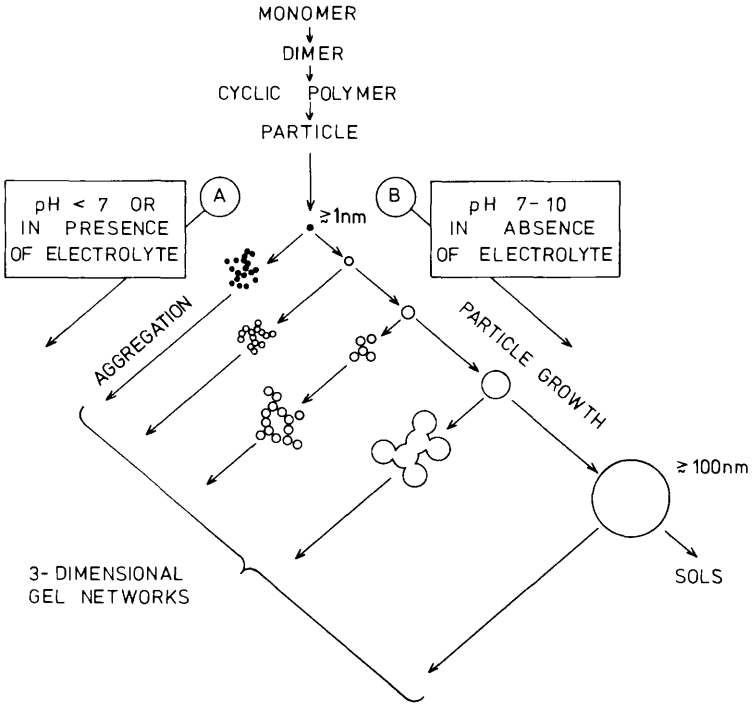

Figure 5 *Schematic illustration of the polymerization of monosilicic acid to form seed particles. In basic solution, (B), these can grow to give sols of different particle size* (viz. *Ostwald ripening*), *whereas at lower pH or in the presence of electrolyte, (A), aggregation occurs, which can lead to the formation of three-dimensional gel networks.*

aggregate and may eventually form a precipitate. These extreme situations are illustrated by the behaviour of silica dispersions as depicted schematically by Iler[19] in Figure 5.

The production of stable concentrated sols of other oxides has been achieved by nucleation and growth processes, by maintaining control of pH and electrolyte concentration. It is inevitably more demanding to obtain concentrated dispersions by these processes because of the high concentration of destabilizing counterions (normally anions) in the system. This problem has been overcome by partially neutralizing salt solutions with amines in a separate immiscible phase. Thus, using long chain tertiary amines [*e.g.* $(C_nH_{2n+1})_3NH_2$, where $n \approx 18$], the extraction of anions from concentrated solutions has been achieved in a controlled manner.[28] An alternative, but less efficient method, involves controlled dialysis of dilute salt solutions followed by a concentration stage using membrane filtration.[38]

Another more general route to concentrated sols is by the peptization of hydrous

oxide precipitates which have been prepared under controlled conditions.[26,54] Referring to Figure 4 it can be seen that the rapid neutralization of a concentrated metal salt solution will cause the solute supersaturation limit to be far exceeded, resulting in the sudden production of a vast number of nuclei which have only a limited possibility for further growth. Such a process will yield a precipitate containing very small amorphous or poorly crystalline particles, typically ~10 nm in size. If washed, to remove excess counterions, such precipitates can be peptized by controlled addition of either a dilute acid or alkali to give a stable concentrated sol containing particles which have a relatively narrow size distribution.

C. The Oxide/Water Interface.—The surface charge and nature of oxide/water interfaces have a dominant effect on the stability and properties of oxide sols. A hydroxylated oxide surface in contact with water can develop either a positive or negative surface charge, as shown schematically in Figure 6. This demonstrates that oxide surfaces have amphoteric properties and that the charge-determining ions are either H^+ or OH^-. The surface charge will consequently be dependent on pH and will vary depending on the type of oxide surface studied.

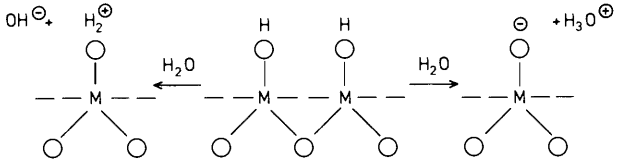

Figure 6 *Schematic illustration of surface charge generation on an oxide surface*

The pH of zero point of charge (z.p.c.), which can be determined by potentiometric titration methods, reflects the acid/base character of the surface; a low z.p.c. corresponds with a more acidic nature, as is the case for silica. Values of z.p.c. for a number of oxides are given in Table 1.

Table 1 *Typical pH values for oxides at the zero point of charge*[55]

Oxide	*z.p.c.*	*Oxide*	*z.p.c.*
WO_3	~0.5	ZrO_2	~5
SiO_2	~2	γ-Al_2O_3	7.5
SnO_2	4.3	α-Fe_2O_3	8.5
TiO_2	~6	CeO_2	6.8
		Co_3O_4	11.4

These are typical values which may vary by one or even two pH units depending on the method of preparation of the oxide and its pretreatment. These variations

[54] J. D. F. Ramsay, S. R. Daish, and C. J. Wright, *Faraday Discuss. Chem. Soc.*, 1978, **65**, 65.
[55] G. A. Parks and P. L. de Bruyn, *J. Phys. Chem.*, 1962, **66**, 967.

probably reflect different surface structures and the presence of adsorbed foreign ions and contaminants. Such factors can have a much more marked effect on the titratable surface charge.

As a result of the charged groups an electrostatic potential, φ_0, is developed at the surface relative to the bulk solution. Furthermore, to retain electroneutrality, ions of opposite charged (counterions) are concentrated close to the surface, whereas the charge-determining ions are depleted in this zone. By assuming a Boltzmann distribution of ions, such a description leads to the familiar diffuse double layer model,[11] in which the potential decreases with the distance from the surface, r, as

$$\varphi(r) = \varphi_0 \exp(-\kappa r) \tag{6}$$

where κ is the Debye–Hückel inverse screening length given by

$$\kappa = \left[\frac{2c_i N e^2 \nu^2}{\varepsilon_0 \varepsilon k T}\right]^{\frac{1}{2}} \tag{7}$$

Here c_i is the ionic strength of the solution, ν the valency of the ions, ε the dielectric constant of the solvent, ε_0 the permittivity of vacuum, N is Avogadro's number, and k the Boltzmann constant. For spherical particles, of radius R say, the surface charge z_p is related to φ_0 by the approximation

$$\varphi_0 = z_p/4\pi\varepsilon\varepsilon_0 R(1 + \kappa R) \tag{8}$$

Colloidal dispersions of oxide particles are in general stabilized by a mutual repulsion resulting from the interaction between their electrical double layers, which overcomes the van der Waals attractive interaction. Since details of lyophobic colloid stability theory have been treated extensively elsewhere[11] this aspect will not be developed further here. However, it will be noted that stability is enhanced when φ_0 is large and $\varphi(r)$ falls away gradually from the surface. The latter situation is favoured when κ^{-1} is large, *i.e.* where c_i is small (*e.g.* $< 10^{-3}$ mol dm^{-3}) and ε large.

In this simple description of the electrical double layer, it is assumed that the ions can be treated as point charges and that the only forces between the surface and counterions are non-specific Coulombic forces. This simplification, although satisfactory for many colloid systems in which the ionic strength is relatively low, ($\lesssim 10^{-2}$ mol dm^{-3}) and where the surface charge density is modest (< 10 μC cm^{-2}), is particularly inadequate for oxide interfaces. This has been widely demonstrated[56,57] by the very large values of surface charge density obtained by titration, which far exceed those derived from electrokinetic measurements. These differences are partly reconciled by the Stern theory[58] which assumes that a layer of

[56] J. Lyklema, in 'Colloidal Dispersions', ed. J. W. Goodwin, Special Publication No. 43, The Royal Society of Chemistry, London, 1982, p. 47.
[57] J. Lyklema, *Croat. Chem. Acta*, 1971, **43**, 249.
[58] O. Stern, *Z. Electrochem.*, 1924, **30**, 508.

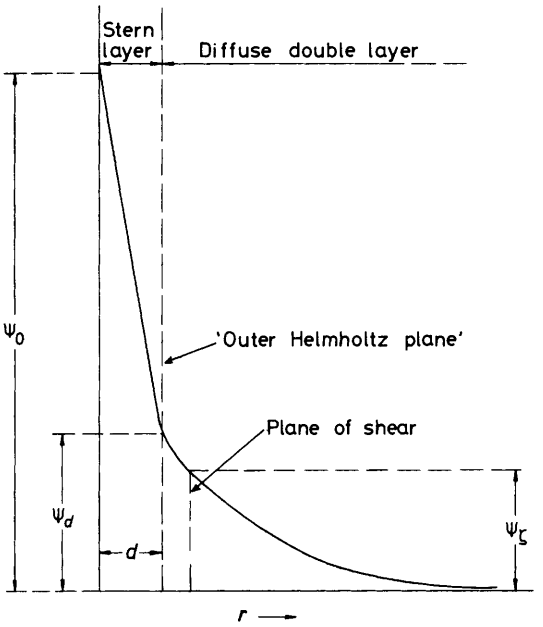

Figure 7 *Schematic diagram of an electrical double layer showing the potential variation with distance, r, from a charged surface*

counterions of finite size is located within a few Ångstroms of the surface, across which the electrical potential falls linearly. This results in the potential distribution shown in Figure 7, where the diffuse double layer starts at a distance d from the surface—the 'outer Helmholtz plane'. The potential at this plane, φ_d, is taken to be close to the zeta potential, ζ, which is measured electrokinetically (*e.g.* by electrophoresis) at the plane of shear.[56] This model makes a tacit allowance for a reduction in the permittivity of the water due to the high field strength very close to the surface, and for specific adsorption forces between the counterions in the Stern layer and the surface.

Even this description often cannot completely explain the very large surface charges and low ζ-potentials of oxides and has led to further refinements such as the site binding model[59] and the 'porous gel' model.[57] The former assumes that direct binding of counterions to surface charges occurs, whereas in the latter it is postulated that H^+ and OH^- ions can penetrate the surface layer of the oxide thus resulting in an enhanced 'surface charge density'. In both of these models neutralization of charge by counterions will occur depending on the polarizing effect of the ion on the water molecules in its hydration shell, compared to that induced by the 'surface' charge. If the latter is stronger, then water of hydration will

[59] R. O. James and G. A. Parks, in 'Surface and Colloid Science', ed. E. Matijevic, Wiley Interscience, New York, 1980, Vol. II.

be lost and the ion will be localized within the surface layer. This would explain why in the lyotropic series Li, Na, K, Rb, Cs,—where the hydration energy decreases with ionic diameter, the Cs^+ ion is more effective than the Li^+ ion in destabilizing silica sols,[19] whose exceptional stability may in particular be ascribed to such a diffuse surface structure.

Such factors as outlined here may take on a greater significance in determining the interaction potential in concentrated colloidal dispersions of oxides, especially where the interparticle separation is small and where the screening parameter will become dependent on the particle volume fraction. In these situations direct determinations of the interaction potential from neutron scattering investigations are of particular importance for providing an insight into the nature of oxide water interfaces, as will be described.

3 The Sol to Gel Conversion

Although the properties of oxide sols are of fundamental interest in colloid science they are also of widespread importance in many areas which range from environmental chemistry[41] (soil science, mineral dissolution) to technological applications in ceramic fabrication which employ sol/gel processes for example.[27,28] In the latter, a concentrated sol is converted into a solid hydrous oxide gel, as depicted schematically in Figure 8.

The structure and interactions in the sol are of considerable interest here, since these may predetermine the rheological behaviour during the conversion process and ultimately the final microstructure of the gel—in particular its surface area and porous properties.[37,60] This feature is illustrated schematically in Figure 9 where gels of low and high porosity are derived from unaggregated and aggregated sols respectively. These contrasting types of sol will be referred to subsequently. Apart from its relevance to this specific application a study of concentrated oxide sols can provide a direct insight into the nature of oxide/water interfaces, and interparticle forces which influence colloid stability. Some of the techniques which have been applied and the information obtainable are summarized in Table 2. Many of these are familiar techniques which have been described extensively elsewhere[2,61] and need not be dealt with here. The application of neutron scattering is, however, a quite recent development in colloid studies and has led to considerable advances in the understanding of concentrated dispersions. The background of this technique and the progress made in its application to studies of oxide sols will therefore be covered in depth in the following sections.

4 General Aspects of Neutron Scattering Techniques

The energy of neutrons used in scattering studies normally falls within the range ~ 300 to ~ 0.4 meV, correspond to a wavelength, λ, between ~ 0.5 to ~ 15 Å.

[60] R. G. Avery and J. D. F. Ramsay, in 'Adsorption and Catalysis on Oxide Surfaces', Vol. 21, ed. M. Che and G. C. Bond, Elsevier, Amsterdam, 1985, p. 149.

[61] See *e.g.* 'Colloidal Dispersions', ed. J. W. Goodwin, Special Publication No. 43, Royal Society of Chemistry, London, 1982.

Figure 8 *Features of the Sol–Gel process*

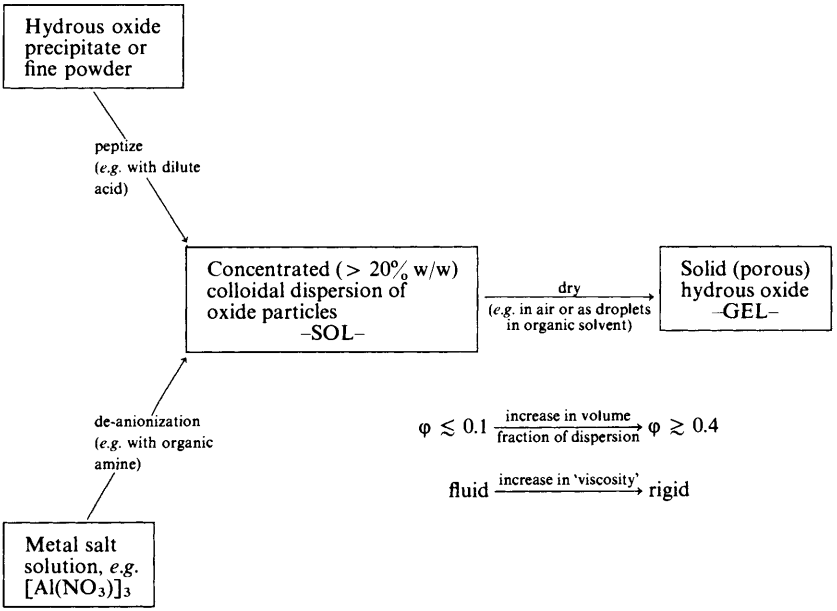

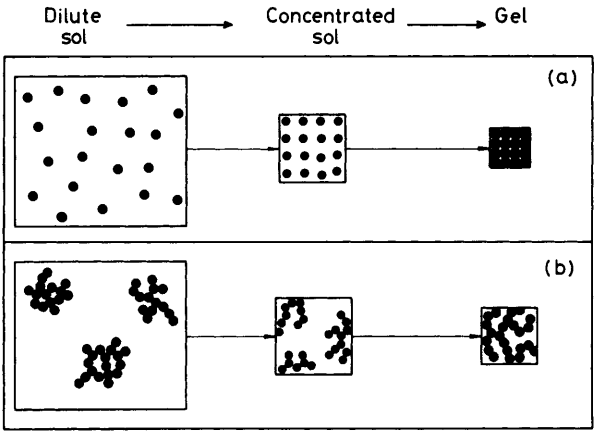

Figure 9 *Diagram depicting the formation of gels of low and high porosity from (a) unaggregated and (b) aggregated sols respectively*

Table 2 *Studies of structure and particle interactions in concentrated oxide dispersions (sols and gels)*

	Technique for Study	*Information*
Sol interactions	Rheology; measurements under steady and oscillatory shear (Weissenberg rheogoniometer)	Flow behaviour of dispersions; particle interactions at high volume fraction
	Microelectrophoresis	Electrophoretic mobility—surface charge
	I.r. spectroscopy	Properties of interfacial water layers—particle interaction
	Inelastic and quasielastic neutron scattering	
Sol structure	Static light scattering	Particle size of sol; MWt and size of sol aggregates (low concentration)
	Quasielastic light scattering (photon correlation spectroscopy)	Diffusional and rotational motion of colloid particles (Surface/solvent interactions)
	Small angle *X*-ray scattering	Particle size of sol; particle ordering at high concentration (radial distribution function); interparticle forces
	Small angle neutron scattering	
Gel structure	Gas adsorption isotherms	Size and arrangement of sol particles on removal of dispersion medium (water); (pore size, pore volume specific surface area)
	Electron microscopy	
	X-Ray line broadening	
	Small angle neutron scattering	

Traditional sources of neutrons have been nuclear reactors, some of which have been designed to produce a high flux within this energy range; typical of these is the high flux reactor (HFR) at ILL, Grenoble.[62] These reactors have more recently been complemented by pulsed sources which employ particle accelerators to generate neutrons by the bombardment of a target, as for example in the Spallation Source, at the Rutherford Laboratory in Oxfordshire.[63]

Neutron scattering by matter arises either through an interaction with the atomic nucleus or magnetically, if atoms have unpaired electron spins. Since detailed treatments of these different scattering processes have been given in numerous reviews and books[64–66] the following outline will only indicate the basic

[62] B. Maier, 'Neutron Research Facilities at the ILL High Flux Reactor', ILL, Grenoble, 1983.
[63] See *e.g.* J. W. White and C. G. Windsor, *Rep. Prog. Phys.*, 1984, **47**, 707.
[64] W. Marshall and S. W. Lovesey, 'Theory of Thermal Neutron Scattering', Oxford University Press, London and N.Y., 1971.
[65] G. E. Bacon, in 'Neutron Scattering in Chemistry', Butterworths, London, 1977.
[65a] S. W. Lovesey, in 'Theory of neutron scattering from condensed matter', Vols. 1 and 2. Clarendon Press, Oxford, 1984.
[66] In 'Chemical Applications of Thermal Neutron Scattering', ed. B. T. M. Willis, Oxford University Press, London, 1973.

principles and information which can be derived from the technique when applied in the present context. In particular we will confine our attention to the more important phenomenon of nuclear scattering.

We can describe the scattering from a single rigidly fixed atom in terms of its cross section, σ, where

$$\sigma = 4\pi b^2 \tag{9}$$

Here b is defined as the scattering length of the bound atom. However, when scattering occurs from matter which is composed of an assembly of non-rigidly bound atoms, there will be two distinct contributions to the total cross section, which arise from coherent and incoherent effects. The first of these, σ_{coh}, results in interference between the neutron waves scattered by the nuclei, and is associated with a coherent cross section given by $\sigma_{coh} = 4\pi b_{coh}^2$. The second, σ_{inc}, is due to interactions between the spin states of the neutron and the nucleus, and gives rise to isotropic scattering; it does not exist for nuclei having zero spin, *e.g.* ^{12}C and ^{16}O.

Values of b_{coh}, σ_{inc}, and the neutron absorption cross section, σ_a, for different nuclei, some of which can occur in oxide sol systems, are given in Table 3. This shows that b_{coh} varies erratically from element to element, and even for different isotopes—a feature which can be exploited in contrast variation studies,[67] as will be described. Another important feature is the large value of σ_{inc} for the proton, which dominates that for other nuclei; this makes incoherent scattering measurements particularly suitable for the study of hydrogenous materials (*e.g.* water, polymers *etc.*), in situations where other spectroscopic techniques are unsuited because of absorption problems.

Table 3 *Coherent scattering lengths,* b_{coh}, *and incoherent and absorption cross-sections,* σ_{inc} *and* σ_a, *for different elements*

	$10^{12}b_{coh}$/cm*	$10^{24}\sigma_{inc}$/cm^2	$10^{24}\sigma_a$/cm^2
H	−0.374	79.7	0.33
D	0.667	2.0	0.0005
C	0.665	0.0	0.0035
N	0.94	0.3	1.9
O	0.58	0.0	0.000 19
Al	0.35	0.0	0.23
Si	0.42	0.0	0.17
Ti	−0.34	3.0	6.1
Fe	0.95	0.4	2.6
Zr	0.72	0.3	0.18
Ce	0.48	0.0	0.63
Th	0.98	0.0	7.4
U	0.842	0.0	7.5

* Data are for natural isotopic mixtures and a neutron wavelength of 1 Å. (As compiled by S. W. Lovesey, *ref.* 65*a*)

[67] B. Jacrot, *Rep. Prog. Phys.*, 1976, **39**, 911.

One of the most important features of neutron scattering compared to other radiation scattering techniques is its ability to probe both the structure and dynamic properties of materials over a wide spatial range extending from about 1 to 10^3 Å as illustrated in Figure 10. For structural studies of colloids and interfaces the upper part of this range is particularly important and overlaps with that covered by small angle *X*-ray scattering (SAXS) and static light scattering (SLS). Furthermore, because of the high energy resolution which is now attainable in neutron scattering, the energy or timescale of dynamic processes that can be studied extends from approximately 10^{-14} s to the region of 1 μs which overlaps with that covered by dynamic light scattering (DLS). This makes the study of diffusion processes in both molecular and colloidal systems possible.

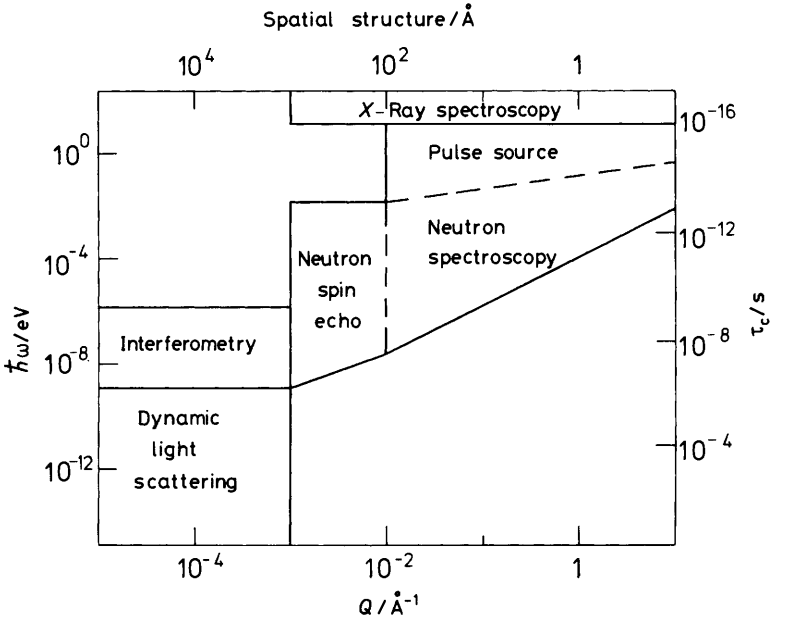

Figure 10 *Energy and spatial resolution of different scattering techniques*

This wide range of timescale, which is equivalent to a correspondingly large energy transfer range as illustrated in Figure 10, has been particularly valuable in the study of incoherent scattering processes. Investigations of water both in the bulk and at interfaces, such as those of clays,[68–70] oxides,[54,71–72a] and polynuclear

[68] S. Olejnik, G. C. Sterling, and J. W. White, *Spec. Discuss. Faraday Soc.*, 1970, **1**, 194.
[69] J. J. Tuck, P. L. Hall, M. H. B. Hayes, D. K. Ross, and C. Poinsignon, *J. Chem. Soc., Faraday Trans. 1*, 1984, **80**, 309.
[70] J. Conard, H. H. Szwarkopf, C. Poinsignon, and A. J. Dianoux, *J. Phys. (Paris)*, 1984, **45**, 169.
[71] J. D. F. Ramsay, H. J. Lauter, and J. Tomkinson, *J. Phys. (Paris)*, 1984, **45**, 73.
[72] J. W. Clark, P. G. Hall, A. J. Pidduck, and C. J. Wright, *J. Chem. Soc., Faraday Trans. 1*, 1985, **81**, 2067.
[72a] C. Poinsignon and J. D. F. Ramsay, *J. Chem. Soc., Faraday Trans. 1*, 1986, **82**, in press.

ions[47,48] for example, are of particular significance here. Although it is not appropriate to consider these further, it has however been shown from inelastic and quasielastic scattering that marked differences in the intermolecular modes and dynamics of water can arise at interfaces. Studies of dynamic processes using quasielastic coherent neutron scattering, although applicable to colloid systems, have been much less. These have included measurements of the diffusion of latex particles and polymers using the recently developed spin-echo technique.[73]

Neutron coherent scattering has its counterpart in small angle *X*-ray (SAXS) scattering and diffraction, for which the theory is very similar,[74] although the possibilities afforded by contrast variation are unique to neutron scattering.[67] Small angle scattering, SAS, arises from variations of scattering length density (see below) which occur over distances d_{SAS} (where $d_{SAS} \simeq \lambda/2\theta$ corresponding to a scattering angle 2θ for radiation with a wavelength λ) exceeding the normal interatomic spacings in solids and liquids.[74,75] Such an effect thus occurs with (i) colloidal dispersions of particles,[33] and polymers in liquids,[73] (ii) assemblies of small particles in air or vacuum comprising a porous material,[74,75,77] and (iii) solid solutions such as alloys.[78]

With many of these systems there are frequently inherent practical advantages in using neutron radiation because of its lower absorption in most materials compared to that of *X*-rays; the latter usually require very thin specimens and considerable restrictions on the sample environment.

In the subsequent sections the application of small angle neutron scattering in studies of concentrated oxide sols will be described at length.

5 Small Angle Neutron Scattering (SANS) Studies of Oxide Sols

The application of SANS to the study of concentrated colloidal dispersions has recently had a considerable impact on our understanding of these systems. Some of the most notable work has been reported by Ottewill and co-workers who have studied monodispersed polystyrene latex dispersions.[30] These developments are timely, because they parallel advances in the application of statistical mechanics to concentrated dispersions which stem from theories of simple liquids.[31]

Typical systems where SANS studies can provide information on structure and interactions are illustrated schematically in Figure 11. We will consider some of these in the foregoing discussion, with a particular emphasis on those typified by (c), (d), and (f). We will consider in particular the recent progress made in the study of concentrated sols composed of small isotropic particles such as silica,[37–40] which being spherical are most suited for such investigations. This will require a

[73] J. S. Higgins, K. Ma, L. K. Nicholson, J. B. Hayter, K. Dodgson, and J. A. Semlyen, *Polymer Vol.*, 1983, **24**, 793.
[74] A. Guinier and G. Fournet, 'Small Angle Scattering of *X*-rays', Wiley, New York, 1955.
[75] G. Kostorz, in 'A Treatise on Materials Science and Technology', ed. H. Herman, Academic Press, New York, p. 227, 1979.
[76] J. S. Higgins, *J. Appl. Cryst.*, 1978, **11**, 346.
[77] B. O. Booth and J. D. F. Ramsay, in 'Principles and Applications of Pore Structural Characterization', ed. J. M. Haynes and P. Rossi-Doria, J. W. Arrowsmith Ltd., Bristol, 1985, p. 97.
[78] V. Gerold, *J. Appl. Crystallogr.*, 1978, **11**, 376.

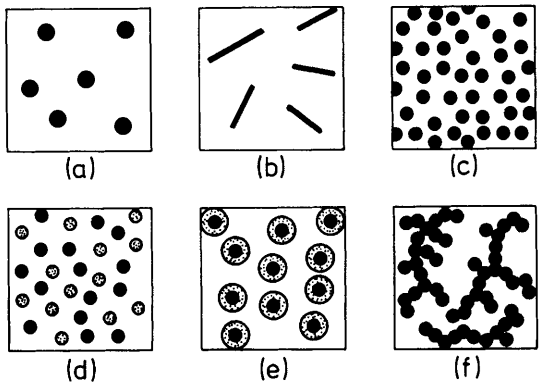

Figure 11 *Schematic illustration of different types of colloidal system which may be studied by small angle neutron scattering: (a) and (b), dilute colloid dispersions of regularly shaped particles; (c) and (d), concentrated dispersions of interacting particles—in (d) there is a two component mixture; (e), dispersion of particles having an adsorbed layer of different scattering length density,* (e.g. *surfactant or polymer molecules); (f), aggregates of particles*

brief description of the theory of SANS, although several more detailed and fundamental treatments can be referred to if necessary.[67,74,75]

A. Theory of SANS.—The scattering of neutrons associated with the coherent cross section of nuclei in a material has a spatial distribution, which is a function of the distribution of these nuclei, and can be expressed as a partial coherent cross section:

$$\frac{d\sigma_{coh}}{d\Omega} = \frac{I_s(\Omega)}{I_0 N} \tag{10}$$

where I_s is the scattered intensity in solid angle Ω (neutron s^{-1} sr^{-1}), I_0 is the incident flux (usually expressed as neutron s^{-1} cm^{-2}), and N the number of scattering nuclei exposed to the beam.

The coherent cross section per atom at small angles 2θ (or small momentum transfer, Q, where $Q = 4\pi\sin\theta/\lambda$) is given in the static or time averaged approximation as:

$$\frac{d\sigma}{d\Omega} = \frac{1}{N}\left[\sum_R b_R \exp(iQ\cdot R)\right]^2 \tag{11}$$

where b_R is the coherent scattering length of the chemical species occupying a site with position vector R in the material, and $\sigma_{coh} = 4\pi\bar{b}^2$. Here the momentum transfer, or scattering vector, Q, is defined as the difference between the wave vectors of the incident, k_0, and scattered neutrons, k:

$$Q = k_0 - k \tag{12}$$

where $k_0 \approx k$.

By replacing b_R by a locally averaged scattering length density $\rho_b(r)$, where r is a variable position vector, we can write

$$\frac{d\sigma}{d\Omega} = \frac{1}{N}\left[\int_V \rho_b(r)\exp(iQ\cdot r)d^3r\right]^2 \tag{13}$$

where the integration extends over the sample volume, V.

For the case of a two-phase system, composed of particles having a homogeneous scattering length density, ρ_p, dispersed in a liquid of scattering density ρ_s equation (13) can be simplified to

$$\frac{d\sigma}{d\Omega} = \frac{1}{N}(\rho_p - \rho_s)^2\left[\int_V \exp(iQ\cdot r)d^3r\right]^2 \tag{14}$$

which describes spatial and orientational correlations and effects due to the size distribution of the particles. If we neglect these effects and assume that the particles are mono-sized, then the integral can be expressed in terms of a single particle form factor, $P(Q)$, given by:

$$P(Q) = \frac{1}{V_p^2}\left[\int_V \exp(iQ\cdot r)d^3r\right]^2 \tag{15}$$

where V_p is the particle volume. Then equation 14 can be written as

$$\frac{d\sigma}{d\Omega} = \frac{V_p^2 N_p}{N}(\rho_p - \rho_s)^2 P(Q) \tag{16}$$

where N_p is the number of particles in the scattering volume V.

A general and convenient method of expressing scattered intensity is in terms of macroscopic cross sections (*i.e.* cross section densities):

$$\frac{d\Sigma}{d\Omega} = \frac{d\sigma}{d\Omega}\frac{N}{V} \tag{17}$$

where N/V is the atomic density of the material. Equation 16 then becomes

$$\left(\frac{d\Sigma}{d\Omega}\right)_{coh} = V_p^2 n_p(\rho_p - \rho_s)^2 P(Q) \tag{18}$$

where n_p is the particle number density. $d\Sigma/d\Omega$ can be expressed on an absolute basis by normalizing scattered intensities against those measured with a water (or

vanadium) standard which has a large incoherent cross section ($[d\Sigma/d\Omega]_{H_2O} = 0.51$ cm ^{1} sr ^{1} at $\lambda = 6$ Å).

The form factor, $P(Q)$, has been evaluated for a variety of particle shapes which include spheres,[79] ellipsoids,[80] cylinders, rods,[74] and flat discs[81] for example. For spheres of radius R, it is given by

$$P(Q) = \frac{3[\sin(QR) - QR\cos(QR)]^2}{Q^3R^3} \tag{19}$$

and is illustrated in Figure 12a. It will be noted that initially the curve decreases exponentially in accord with the Guinier equation:[74]

$$P(Q) \approx \exp(-Q^2R_g^2/3) \tag{20}$$

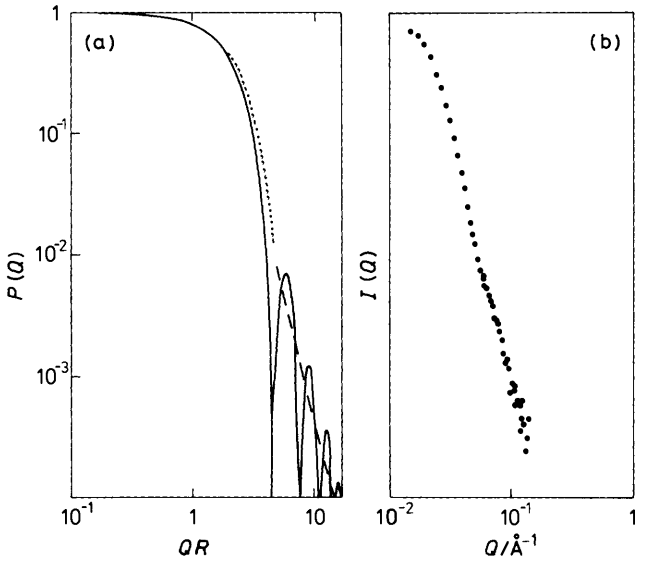

Figure 12 *(a) Form factor, $P(Q)$ for a spherical particle of radius, R. .... corresponds to exponential decay which shows departure from $P(Q)$ at $QR > 1$; – – – corresponds to decay as Q^{-4}. (b) SANS from a dilute* (0.014 g cm^{-3}) *silica sol of particle size* ≈ 16 nm

This is a general relationship, which is valid for all particle shapes, and describes the decay of $P(Q)$ in terms of the radius of gyration, R_g, of the particle in a range $QR_g \lesssim 1$. (*N.B.* for spheres $R = 1.29\ R_g$). At higher Q, ($QR \gtrsim 4$), $P(Q)$ oscillates about a line which decays as Q^{-4}—which is predicted by the Porod law,[81] *viz.*

[79] Lord Rayleigh, *Proc. R. Soc. London*, 1914, **A90**, 219.
[80] A. Guinier, *Ann. Phys.*, 1939, **12**, 161.
[81] O. Kratky and G. Porod, *J. Colloid Sci.*, 1949, **4**, 35.

$$P(Q) \propto (S/V)Q^{-4} \tag{21}$$

where (S/V) is the surface to volume ratio of the particle.

The higher maxima in $P(Q)$ for spheres are only observed experimentally when the colloidal particles are highly monodispersed and the neutron beam well monochromated. This departure from the theoretical curve is demonstrated in Figure 12b by the typical results for a dilute silica sol containing approximately spherical particles with a diameter of ~ 16 nm and a polydispersity of $\sim 20\%$. The effects of polydispersity on the form of $P(Q)$ have indeed been analysed extensively, particularly for spherical particles,[82] and as would be expected slight polydispersity tends to 'smear out' the maxima (see Figure 12b).

B. Structure Determinations in Concentrated Sols

Equation 18 is only valid for dilute dispersions containing widely separated non-interacting particles, where scattered intensity is proportional to the intensity relative to a single particle. In more concentrated dispersions, the intensity distribution is modified by the effects of interference, which depend on the spatial ordering of the particles. The scattered intensity is then

$$\left(\frac{d\Sigma}{d\Omega}\right)_{coh} = V_p^2 n_p (\rho_p - \rho_s)^2 P(Q) S(Q) \tag{22}$$

where $S(Q)$ is the static structure factor, which is determined by the nature of the particle interaction potential; for non-interacting systems $S(Q) = 1$ (*cf.* equation 18.) The spatial distribution of the particles as a function of the mean interparticle separation, r, is given by the particle pair-distribution function $g(r)$ and is related to $S(Q)$ by the Fourier transform

$$g(r) - 1 = \frac{1}{2\pi^2 n_p} \int_0^\infty [S(Q) - 1] Q^2 \frac{\sin(QR)}{QR} dQ \tag{23}$$

Using this type of analysis the structural changes which occur during the progressive concentration and conversion of sols into gels has been investigated for several oxide systems.[37,38] Results for silica and ceria sols in Figures 13 and 14 illustrate the dependence of scattered neutron intensity, $I(Q)$, on momentum transfer, Q, for a range of concentrations. At the lowest concentration there is a gradual decrease in $I(Q)$, which has a form expected (*via* equation 19) for discrete non-interacting particles having diameters in close agreement with those determined from electron microscopy (*ca.* 16 and 7 nm respectively). The development of the maxima in $I(Q)$ at higher concentrations is caused by interference effects and indicates that the particles are not arranged at random but have some short-range ordering due to interparticle repulsion. Thus the movement of the maxima to higher values of Q with increasing sol concentration reflects a reduction in the equilibrium separation distance, $r_{g(r)max}$, $(= r^*)$ between the

[82] A. Vrij, *J. Colloid Interface Sci.*, 1982, **90**, 110.

particles. The form of $g(r)$, which defines the probability that the centres of a pair of particles will be separated by a distance r, is typified by results for silica sols shown in Figure 15. An insight into the structural changes which occur in converting sols into gels can be obtained from the dependence of r^* on the sol concentration, c.

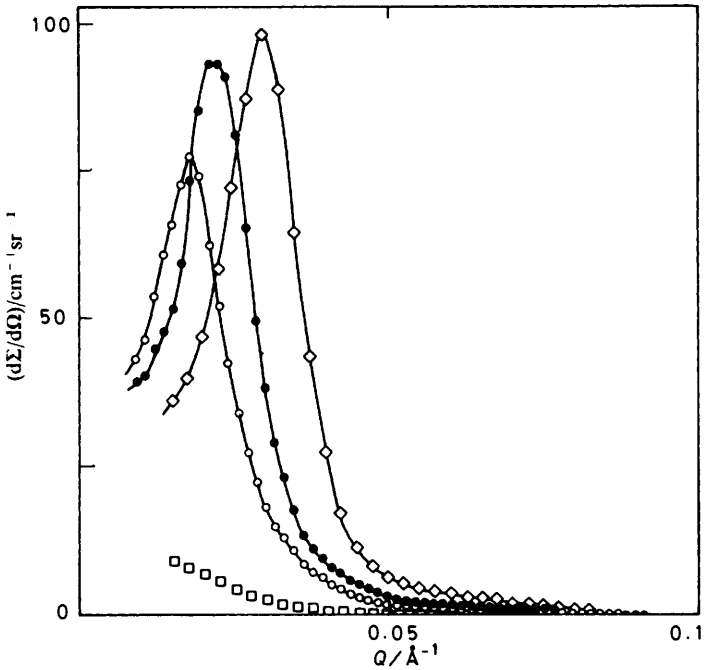

Figure 13 *Small angle neutron scattering from silica sols of different concentrations, c:* □, 0.014; ○, 0.14; ●, 0.27; *and* ◇, 0.55 g cm^{-3}. *Particle diameter is* ~16 nm (Reproduced from *Faraday Discuss. Chem. Soc.*, 1983, **76**, 53)

In general it is found that as c is increased the interparticle separation decreases inversely as $c^{1/3}$ and approaches that of the particle diameter, $2R$, as the solid gel is formed. This feature, which is illustrated by results for ceria and silica sols in Figure 16, indicates that there is little change in the relative arrangement of particles when the volume fraction is increased by over an order of magnitude. The absence of a discontinuity in these plots also implies that in the conversion of sols into gels there is no abrupt change from short- to long-range order (*viz.* order–disorder transition),[83] as occurs in the freezing of a liquid to a solid having a b.c.c. or f.c.c. structure for example.

An indication of the arrangement of particles in both the sols and gel can also be obtained from the plots of $g(r)$ against r. Thus the average number of nearest neighbours, Z, is obtained from the relationship

[83] B. J. Alder and T. E. Wainwright, *Phys. Rev.*, 1962, **127**, 359.

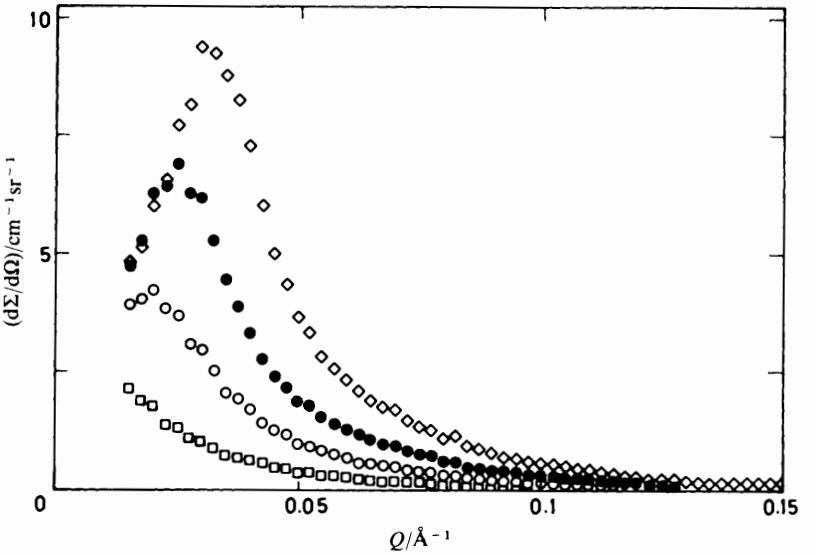

Figure 14 *Small angle neutron scattering from ceria sols of different concentrations, c*: □, 0.032; ○, 0.08; ●, 0.27; *and* ◇, 0.32 g cm^{-3}. *Particle diameter is* ~7 nm
(Reproduced from *Faraday Discuss. Chem. Soc.*, 1983, **76**, 53)

$$Z = 8\pi n_p \int_0^{r^*} r^2 g(r) dr \qquad (24)$$

where r^* is again the position of the first maximum in $g(r)$. From such a procedure it has been shown that values of Z are in general close to 8—a number remarkably similar to that found for simple liquids.[84] Such a large value implies that the particles are packed relatively efficiently when the gel is formed, as is depicted schematically in Figure 9a. A dense particle packing has also been demonstrated by the low porosities and pore sizes of the dehydrated gels which have been determined by nitrogen adsorption isotherm measurements.[37,60] These are in close accord with a random close packed structure having a porosity, ε, of approximately 0.36.

C. Interaction Behaviour in Concentrated Sols

A major aim of current research on concentrated colloidal dispersions is to improve our understanding of interparticle interactions. From such a knowledge of multibody interactions at a microscope level a more confident prediction and

[84] J. S. Rowlinson and C. F. Curtiss, *J. Chem. Phys.*, 1951, **19**, 1519.

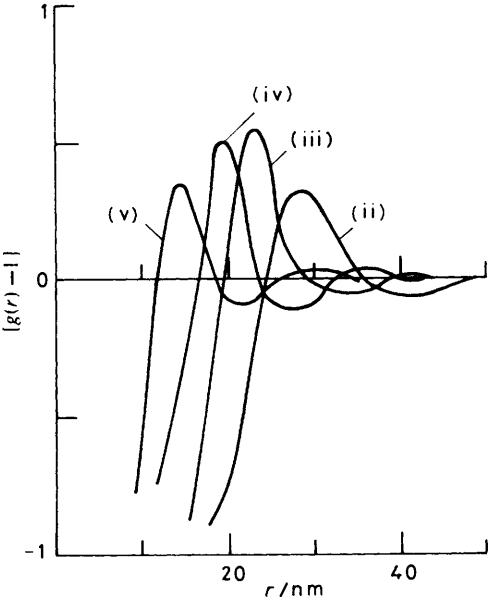

Figure 15 *Radial distribution functions, g(r), for silica sols and gel of different concentrations* (*g cm*$^{-3}$). (ii) 0.16, (iii) 0.41, (iv) 0.65, *and* (v) *ca.* 1.2. *Particle diameter* ~16 nm (Reproduced from *J. Chem. Soc., Faraday Trans. 1*, 1983, **79**, 173)

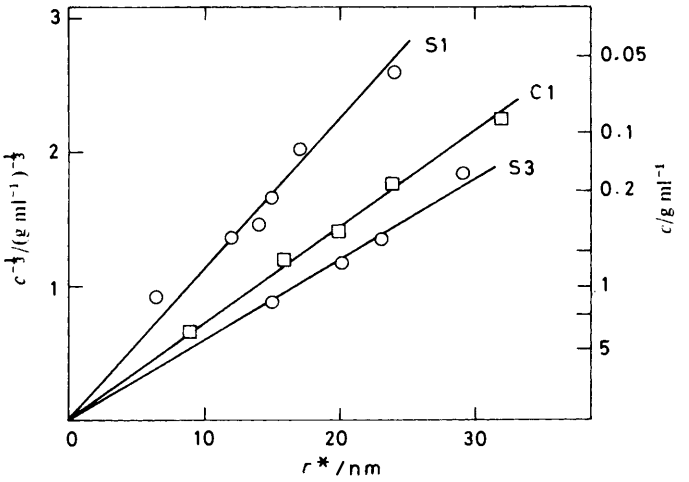

Figure 16 *Dependence of* $r_{g(r)max}$ (= r^*) *on the concentration, c, of silica* (S1 *and* S3) *and ceria* (Cl) *sols and gels. Particle diameters are* ~8, 16, *and* ~7 nm *for* S1, S3, *and* Cl *respectively* (Reproduced from *J. Chem. Soc., Faraday Trans. 1*, 1983, **79**, 173)

control of many macroscopic properties, such as the rheology and stability of dispersions, should be possible. A direct insight into the interaction behaviour can be obtained from the form of $S(Q)$. Particular progress has been made from the analysis of SANS from monodispersed latex particles,[36,85] surfactant micelles,[86] and silica sols[38,39] by modelling the behaviour of the dispersion as a one-component fluid of colloidal particles.[87,88] This approach has been based on established liquid-state models which involve either computer simulation[88,89] or, more frequently, integral-equation methods.[90] Using the latter approach, the behaviour of oxide sol systems has been modelled using the hard-sphere (HS) potential and more recently a screened Coulombic potential using the solution of the rescaled mean spherical approximation (MSA), as developed by Hayter *et al.*[91,92]

The HS potential is a theoretical interaction for assemblies of 'hard spheres', which is now well established[93] as a very satisfactory model for describing the properties of simple liquids, such as liquid argon. In this model, where the particle is regarded as a non-attracting rigid sphere of diameter σ, the potential energy is defined as (see Figure 17a):

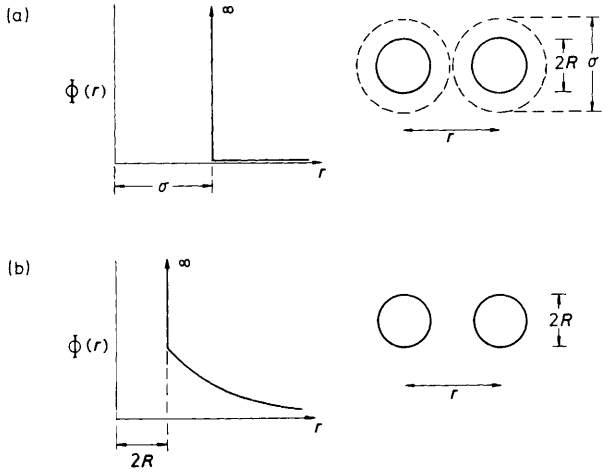

Figure 17 *Schematic illustration of form of repulsive interaction potential, $\Phi(r)$ between spherical particles of radius R separated by a distance, r. (a) Hard-sphere potential; σ is the effective HS. diameter. (b) Hard-sphere potential with 'soft' tail corresponding to DLVO potential*

[85] B. Beresford-Smith and D. Y. C. Chan, *Faraday Discuss. Chem. Soc.*, 1983, **76**, 65.
[86] J. B. Hayter and J. Penfold, *J. Chem. Soc., Faraday Trans. 1*, 1981, **77**, 1851.
[87] J. B. Hayter, *Faraday Discuss. Chem. Soc.*, 1983, **76**, 7.
[88] W. van Megen and I. Snook, *J. Chem. Phys.*, 1977, **66**, 813.
[89] E. Dickinson, *Faraday Discuss. Chem. Soc.*, 1978, **65**, 127.
[90] E. Dickinson, *Annu. Rep. Prog. Chem., Sect. C, Phys. Chem.*, 1983, **80**, 3.
[91] J. B. Hayter and J. Penfold, *Mol. Phys.*, 1981, **42**, 109.
[92] J. P. Hansen and J. B. Hayter, *Mol. Phys.*, 1982, **46**, 651.
[93] J. P. Hansen and I. R. McDonald, 'Theory of Simple Liquids', Academic Press, London, 1976.

$$\Phi(r) = \infty, \quad r < \sigma$$
$$\Phi(r) = 0, \quad r > \sigma \tag{25}$$

It has been shown[38] that the experimental $S(Q)$ for sols of different concentration can be quite closely simulated by that calculated using the Percus–Yevick approximation[94,95] for an assembly of hard spheres, in which σ is dependent on the concentration of both the sol and electrolyte. Thus, for dilute sols of low electrolyte concentration, σ is considerably larger than the real particle diameter, but as the sol concentration is increased during the conversion into the gel, σ progressively decreases. Furthermore, the effective volume fraction, φ_{HS}, of the more dilute sols is relatively large and does not increase greatly as the sol concentration is increased. These features are illustrated in Figure 18 by results obtained with silica sols.

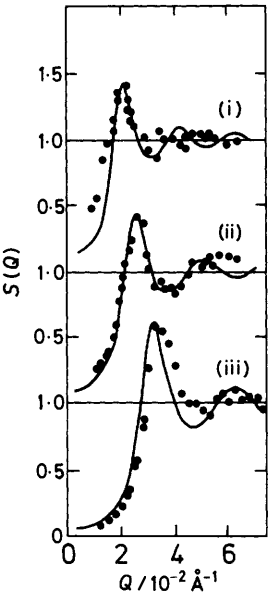

Figure 18 *Structure factors, S(Q), for silica sols of different concentration, c*; (i) 0.14; (ii) 0.27, *and* (iii) 0.55 g cm^{-3}. *Ionic strength,* $c_1 \approx 5 \times 10^{-3}$ mol dm^{-3}. *Particle diameter is* ~ 16 nm. *Full lines correspond to S(Q) for HS systems with* φ_{HS} *of* 0.27, 0.28, *and* 0.32 *for* (i), (ii), *and* (iii) *where* σ_{HS} *is* 31, 25, *and* 20 nm *respectively*

The simple HS model does not however give a completely satisfactory simulation with the experimental $S(Q)$, which is not unexpected because a more slowly decaying potential would be expected to result from the interaction between the electrostatic double layers surrounding the particles. This becomes evident at lower

[94] J. K. Percus and G. J. Yevick, *Phys. Rev.*, 1958, **110**, 1.
[95] N. W. Ashcroft and J. Lekner, *Phys. Rev.*, 1966, **45**, 33.
[96] B. Beresford-Smith, D. Y. C. Chan, and D. J. Mitchell, *J. Colloid Interface Sci.*, 1985, **105**, 216.

sol concentrations where the more gradual increase in $S(Q)$ which occurs initially is an indication that a 'softer' potential would be more suitable for simulation.

This has been demonstrated using the MSA model which gives a closed analytical solution to $S(Q)$ as a function of several parameters of the system defining the interparticle potential, which include the volume fraction, φ_p, the surface charge, and screening, κ. The form of the potential, between the spherical particles is now defined by a hard core potential and the Standard Coulombic potential due to the mutual interaction of their electric double layers:

$$\begin{aligned} \Phi(r) &= \infty, \quad r < 2R \\ \Phi(r) &= 4\pi\varepsilon_0\varepsilon R^2\varphi_0{}^2\exp[-\kappa(r - 2R)]/r, \quad r > 2R \end{aligned} \tag{26}$$

Here the terms are as earlier defined (p. 343) and κ is again the Debye–Hückel inverse screening length. The form of this potential is illustrated schematically in Figure 7b, where now the hard core-diameter will correspond to the actual particle diameter, $2R$.

The application of this model is illustrated in Figure 19 by results obtained with silica sols having three different concentrations but similar pH (*ca.* 8). Here the structure factor $S(Q)$ has been calculated as described previously[39] and the product $KP(Q)S(Q)$, where K contains the terms remaining in equation 22, has been fitted to the experimental data. The effective surface potentials, φ_0 corresponding to the fitted $S(Q)$ at each sol concentration are given in Figure 19. It is well known that the surface of silica has a negative charge which increases gradually with rising pH, as is demonstrated in Figure 20 by the laser electrophoresis results obtained with the same silica sol at much lower concentration. This dependence of surface charge on pH is also reflected in changes in the scattering behaviour of more concentrated sols

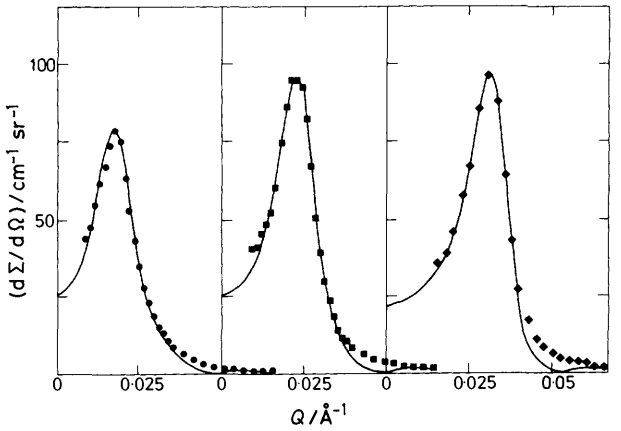

Figure 19 *Small angle neutron scattering of silica sols (diameter* ~16 nm) *of different concentrations dialysed against* 5×10^{-3} mol dm^{-3} *sodium nitrate solution:* ●, 0.14; ■, 0.27; *and* ◆, 0.55 g cm^{-2}. *Continuous lines are the MSA model theoretical fits to the data, and correspond to values of* φ_0 *of* 28, 26, *and* 19 mV *respectively*

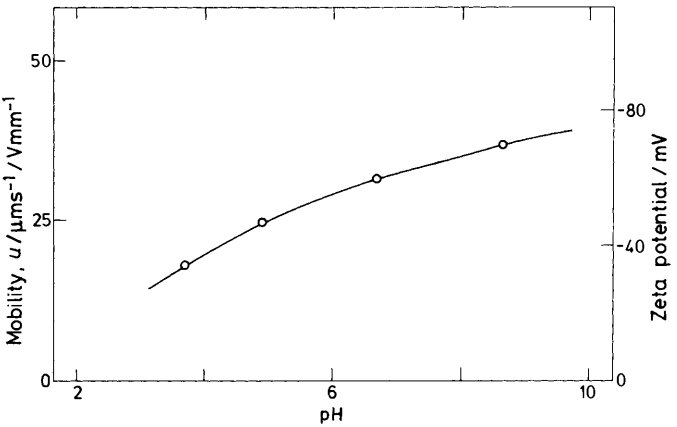

Figure 20 *Dependence of electrophoretic mobility, u, and zeta potential, ζ, on pH for a dilute* ($< 10^{-2}$ g cm^{-3}) *silica sol* ([Na^+] $\approx 10^{-4}$ mol dm^{-3})

as shown in Figure 21. Thus at pH values of 7.2 and 4.5 for example, the sharper peak obtained at the higher pH indicates a stronger repulsive interaction, which arises from a greater effective surface charge, as is confirmed by the φ_0 values of 22.9 and 13.7 mV obtained from the model fits.

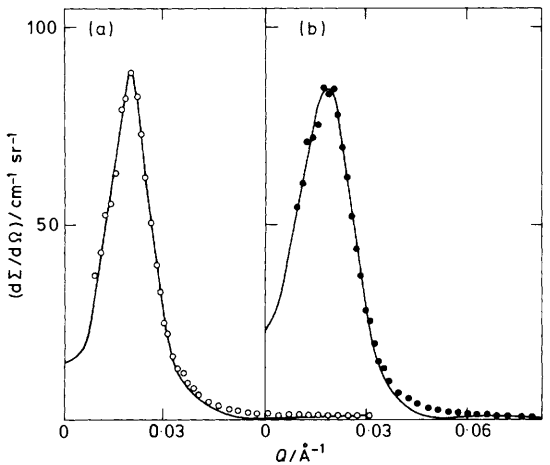

Figure 21 *I(Q) plotted against Q for silica sols of similar concentrations* (*ca.* 0.19 g cm^{-3}) *but different pH,* (*a*) 7.2 *and* (*b*) 4.5, *both dialysed against* 10^{-4} mol dm^{-3} *sodium nitrate. Corresponding values for* φ_0 *are* 14 *and* 23 mV *respectively*

Although the changes in the interaction potential obtained from the MSA model, reflect the effects of changing pH on the zeta potential, the latter are nevertheless significantly larger. This difference may arise because electrophoresis measurements are of necessity restricted to much less concentrated sols as previously discussed.[39] Thus at large volume fractions, the pair potential may be altered for several reasons which include changes in the chemical potential of the dispersion phase, through changes in the particle surface charge density or potential,[88] and the effects of additional screening due to the compensating increase in the counterion concentration[85,96] associated with the particles. Although the latter effect can be allowed for[39] it is particularly significant at high volume fractions of small particles ($\lesssim$20 nm) having a high charge density. Another possible reason for the discrepancy between surface potentials obtained from model fits and the experimental measurements which cannot be overlooked concerns the assumptions inherent in the MSA model, in particular the use of the Debye–Hückel potential to describe double-layer interactions and the extension of the pairwise additivity approximation to describe multibody interactions. Consequently while the application of the Hansen–Hayter MSA form for $S(Q)$ is a useful approach for displaying trends in potential parameters, as illustrated here and in more recent studies of the temperature dependence of interaction forces, it may have limitations in providing absolute values.

D. Studies of Mixed Oxide Sols.—An application where the sol/gel process has a particular advantage is in the preparation of mixed oxide gels, (*e.g.* for glass precursors, catalysts, pigments, electroceramics). Such applications are, however, in general technically more demanding because they require the compatibility of concentrated mixtures of sols, in respect to stability and rheology for example. In principle an understanding of the interactions and homogeneity of the different components in mixed oxide sols may be obtained from SANS by exploiting the contrast variation technique, which has been employed extensively in the study of biological structures.

Such an application has been demonstrated recently with mixtures of iron hydroxide and titania sols.[38,97] These oxides have a large difference in scattering length density, ρ_{oxide}, (see Table 4), and thus under contrast match conditions for one component the scattering from the other is still considerable. This feature is important experimentally, particularly with the very small colloidal particles ($\lesssim$10 nm) which have been studied, because $I(Q)$ is relatively weak (*cf.* equation 22).

The effect of solvent contrast on the scattering of these oxide sols is illustrated by the measurements of $I(Q)$ against Q for samples having different H_2O/D_2O solvent ratios in Figure 22. For titania (Figure 22a) a contrast match was obtained at *ca.* 50 volume % D_2O (data had poor statistics and are not shown) corresponding to a scattering length density, ρ_{TiO_2}, of 2.9×10^{10} cm^{-2}. Because this is significantly

[97] J. D. F. Ramsay and J. Penfold, Institut Laue Langevin Annual Report 1984, Exp. No. 9-09-13, ILL, Grenoble, p. 448.

Table 4 *Molecular scattering lengths,* $\Sigma_i b_i$ *for different oxides and corresponding scattering-length densities,* ρ, *for mass densities,* δ

Oxide	$\Sigma_i b_i/10^{-12}$ cm	δ/g cm^{-2}	$\rho/10^{10}$ cm^{-2}
H_2O	−0.168	1.00	−0.56
D_2O	1.914	1.10	6.36
SiO_2	1.575	2.20	3.47
CeO_2	1.642	7.13	4.10
TiO_2	0.825	3.84	2.39
FeOOH	1.737	4.28	5.04
FeOOD	2.778	4.28	7.96

larger than the calculated value of 2.39×10^{10} cm^{-2} for bulk anatase (*cf.* Table 4) it has been suggested that the sol particles contain protons, possibly as hydroxyl groups, which are readily exchangeable. The contrast match condition for the iron hydroxide sol is not reached even at 100% D_2O (Figure 22b), although from an extrapolation of plots of $I(Q)^{\frac{1}{2}}$ against $\rho_{solvent}$ it was shown that this would be *ca.*

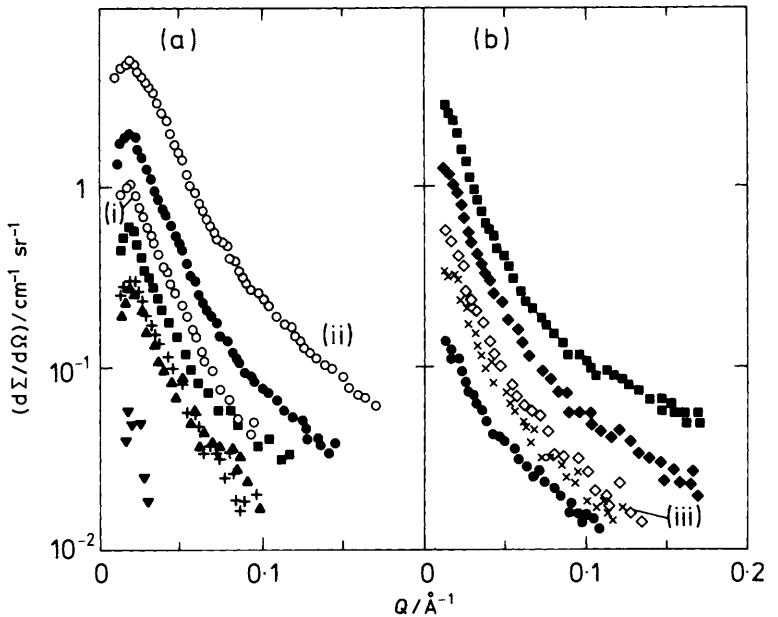

Figure 22 *SANS results for (a) titania and (b) iron hydroxide sols and their mixtures in water with different* H_2O/D_2O *volume fractions. (a) Titania (ca.* 0.028 g cm^{-3}*), volume %* D_2O: ■, 0; ▲, 20; ▼, 40; +, 70, ●, 100; *(i) and (ii) mixed sols* (100% D_2O *with concentrations* (TiO_2 + FeOOH) *of* (0.014 + 0.015) *and* (0.11 + 0.12) g cm^{-3}, *respectively. (b) Iron hydroxide (ca.* 0.030 g cm^{-3}), vol% D_2O: ■, 0; ◆, 50; ×, 80; ●, 100; (iii) *mixture* (50% D_2O) *concentrations as in* (i)

8.4×10^{10} cm^{-2}. This is close to that calculated for α-FeOOD and is an indication that exchange of structural protons occurs readily.

The form of the scattering curve of the titania sol, which can be ascribed to a dispersion containing very small polydispersed spherical particles (diameter 6—8 nm), remains unchanged when the titania and FeOOH sols are mixed [*cf.* Figure 22a, (i) and (ii)]. This shows that the dispersions are mutually stable, probably because both oxides are positively charged at the pH of *ca.* 3 in this system. An interparticle separation of *ca.* 30 nm can be estimated from the position of the interference maximum observed at *ca.* 1.9×10^{-2} Å^{-1} for the titania sol. The slight shifts in this maximum with the mixed sols (*ca.* 1.6×10^{-2} and 2.2×10^{-2} Å^{-1} respectively) show that the separation between the titania particles is still dependent on their number concentration in the presence of the iron hydroxide sol particles. It will also be noted that the form of the scattering from the α-FeOOH sols (Figure 22b) is similar to that of the mixed system [Figure 22b, (iii)], showing there is no heterocoagulation occurring. In more extensive investigations[97] on mixed titania iron oxide sols, prepared with a similar particle size (~10 nm), the scattering has been analysed using the MSA model for the condition of contrast match for the two components. This analysis has given details of $S(Q)$, $g(r)$, and effective surface potential. Evidence of short range order and homogeneous dispersion for iron oxide (TiO_2 matched) in these systems is illustrated in Figure 23 from S(Q) and P(Q) derived from MSA fits.

E. Studies of Sols containing Particle Aggregates

In our discussion up to now we have considered the application of SANS in the study of structure and interactions in sol systems containing discrete almost spherical particles which are nearly monodispersed. Another more complex system

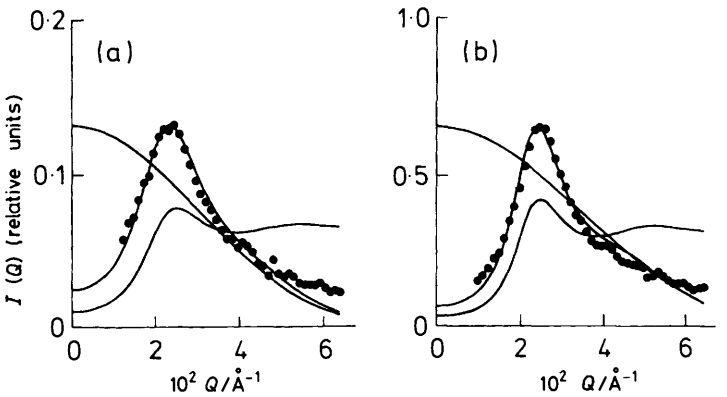

Figure 23 *Small angle neutron scattering results for* (*a*) *a mixed iron hydroxide* (0.027 g ml^{-1}) *titania* (0.044 g ml^{-1}) *sol in* 50% H_2O/D_2O *and* (*b*) *the iron hydroxide sol* (0.051 g ml^{-1}) *above in* 100% H_2O *of similar pH and ionic strength. Full lines correspond to P(Q) and S(Q) from MSA fits*

occurs where the sol is composed of aggregates of primary particles having a diameter somewhat similar to those already considered. A colloidal dispersion of this type can be prepared either by aggregating discrete sol particles[54] or by dispersing pyrogenic oxide (*e.g.* silica, alumina) powders in water[98] for example and is depicted schematically in Figure 9b.

Dispersions of this type are typical of a wide range of colloid systems occurring as flocs and particle clusters, which are important in a variety of natural and commercial processes. The importance of such systems has indeed stimulated considerable efforts to define floc structure, particularly in terms of computer simulations which model flocculation processes.[99–102] The assessment of these models has, however, been difficult, due mainly to a lack of suitable techniques which can probe floc structure. It has, however, been demonstrated recently that the properties of such aggregates can be determined from scattering measurements and thence defined in terms of fractal structure.

This approach for defining the structure of particle aggregates is based on the concept of the fractal dimension,[103] D, and has been developed theoretically using computer simulations of aggregate formation.[101,102,104] Aggregates so formed have the property of self-similarity. That is, the gross structure of the aggregate is the same on length scales greater than that of the range of interaction between the individual particles within the aggregate.

The Hausdorff or fractal dimension, D, of an object can be defined as:

$$N(r) = N_0 r^D \tag{27}$$

where $N(r)$ is the mass contained in a radius r about any point in the object, and N_0 is a constant. For the case of a solid mass for example, $D = 3$ and N_0 is $4\pi/3$. Furthermore, for this simple case, D, and the Euclidian dimension, d, of free space will be identical (*viz.* $D = d$). However, for fractal objects, such as aggregates of spherical particles, $D < d$. For these the density–density correlation function is scale invariant and obeys the relationship:

$$\langle \rho(r' + r)\rho(r') \rangle \sim r^{-A} \tag{28}$$

where the exponent A is given by

$$D = d - A \tag{29}$$

This non-integral dimensionality, d, thus implies that the average density of particles in an aggregate will decrease as the volume sampled is increased. In effect

[98] J. D. F. Ramsay and M. Scanlon, *Colloids and Surfaces*, 1986, **18**, 207.
[99] M. J. Vold, *J. Colloid Sci.*, 1963, **18**, 684.
[100] D. N. Sutherland, *J. Colloid Interface Sci.*, 1967, **25**, 373.
[101] T. A. Witten and L. M. Sander, *Phys. Rev. B*, 1983, **27**, 5686.
[102] P. Meakin, *Phys. Rev. A*, 1983, **27**, 1495.
[103] B. B. Mandelbrot, 'Fractals, Form, Chance and Dimension', W. H. Freeman, San Francisco, 1977.
[104] S. R. Forrest and T. A. Witten, *J. Phys. A., Math. Gen.*, 1979, **12**, 109.

it can be shown that the average number of particles, $N(a)$, within a volume of radius, a, say, will vary as a^D, which is expressed as

$$a^D \sim N(a) = \int_0^a d^3r\langle\rho(r)\rho(0)\rangle/\langle\rho(0)\rangle \tag{30}$$

This expression defines the fractal dimension, D, in terms of the ensemble average density function given by

$$g(r) = \langle\rho(r')\rho(r' + r)\rangle/\rho(r') \tag{31}$$

where $\rho(r')$ is the density at position r'.

It also follows that

$$g(r) \sim r^{(D-d)} \tag{32}$$

It can furthermore be shown that the scattered amplitude [or intensity, $I(Q)$] is given[74] by the general expression:

$$I(Q) \sim \int 4\pi r^2 g(r) \frac{\sin(Qr)}{Qr} d^3r \tag{33}$$

such that $I(Q)$and $g(r)$ are related by a Fourier transform.

It thus follows that $I(Q)$ will also obey a corresponding power law relation given by:

$$I(Q) \sim Q^{-D} \tag{34}$$

Evidently equation 34 will only apply for a certain range of length, r, which for aggregates will be approximately between the diameter of the individual particles and the overall size of the aggregate. Correspondingly the fractal power law observed from scattering measurements (*viz.* equation 34) will hold for a range of Q, which is determined in reciprocal space by these limiting values of r. For small r, comparable with the primary particle size (*viz.* high Q), the power law expected would then be dominated by surface fractal structure. Thus for scattering samples composed of two components (such as aggregates of particles dispersed in a liquid, and porous solids) which are separated by a smooth interface it can be shown that[105]

$$I(Q) \sim S{\cdot}Q^{-(6-D)} \tag{35}$$

where S is the surface area of the interface and D is the surface fractal dimension of 2. This leads to the familiar Porod law relation[81,106]

[105] H. D. Bale and P. W. Schmidt, *Phys. Rev. Lett.*, 1983, **53**, 596.
[106] G. Porod, *Kolloidn. Zh.*, 1951, **124**, 83.

$$I(Q) \sim S \cdot Q^{-4} \tag{36}$$

In certain extreme cases,[105,107] however, where the surface is irregular, or has curvature on a scale smaller than reciprocal Q space, D may become greater than 2. This can lead to power law exponents in equation 36 which are smaller than -4. Such a situation may arise with very small colloidal particles (diameter $\lesssim 100$ Å) as have been demonstrated here.[98,105]

Experimental measurements of scattering from colloidal aggregates or clusters of particles in aqueous dispersions may thus in principle provide an insight into the uniformity, size, and openness of their structure, as will be subsequently demonstrated. The latter feature is implicit in equation 30 which leads to the relationship between the radius of gyration, R_g, of a cluster containing N_c particles:

$$N_c \sim R_g^D \tag{37}$$

Differences in D which reflect the openness of aggregates have indeed been demonstrated by computer simulations, where two idealized models have been considered. Thus for the case of diffusion-limited aggregation (DLA), Meakin[102] has derived a value of D of 2.5, whereas for a situation involving the aggregation of clusters of comparable size (CA) a dimensionality, D, of ~ 1.75 is obtained.[108]

The fractal dimensions of several particle aggregate systems have been determined experimentally either by direct microscopic observation in 2-dimensions ($d = 2$) or more recently by radiation scattering measurements. The structure of aggregates formed from colloidal gold particles have been studied[109,110] in detail using both of these methods and are in close accord. Thus from electron microscopy a D of 1.8 ± 0.1 (in 3-dimensions) has been reported which is in close agreement with that of 1.7 found from light scattering and SANS.

The process of aggregation of discrete Ludox®, silica particles which results from the addition of destabilizing electrolyte has also been studied using a combination of light scattering and small angle neutron scattering,[111] thus covering a wide range in reciprocal space, Q. In such measurements which have been restricted to dilute dispersions because of multiple scattering and attenuation problems as previously described, it has been shown that colloidal aggregates have a fractal dimension of ~ 2.1, which is intermediate between that predicted by the DLA and CA models.

A combination of light scattering and SANS has also been used to investigate colloidal dispersions of pyrogenic silica and alumina.[98] We will describe these results in more detail, first because they illustrate some of the features already

[107] J. K. Kjems and P. Schofield, in 'Scaling Phenomena in Disordered Systems' ed. R. Pynn and A. Skjeltorpe, Plenum Ltd., 1985, p. 141.
[108] M. Kolb, R. Botet, and R. Julien, *Phys. Rev. Lett.*, 1983, **51**, 1123.
[109] D. A. Weitz, J. S. Huang, M. Y. Lim, and J. Sung, *Phys. Rev. Lett.*, 1984, **53**, 1657.
[110] D. A. Weitz and J. S. Huang, in 'Kinetics of Aggregation and Gelation' ed. F. Family and D. Landau, North Holland, Amsterdam, 1984, p. 19.
[111] D. W. Schaefer, J. E. Martin, P. Wiltzius, and D. S. Cannell, *Phys. Rev. Lett.*, 1984, **52**, 2371.

discussed, and secondly because they provide an insight into the process by which a porous gel is formed from such a system on dehydration.

The scattering behaviour of these dispersions are typified by those shown for two different concentrations of pyrogenic silica (Aerosil 200) in Figure 24 (i) and (ii). In both of these $I(Q)$ decays with power law of $Q^{-3.9}$ above a Q of $\sim 2.5 \times 10^{-2}$ Å^{-1}. Such a decay corresponds closely to that of the Porod law, discussed earlier, and demonstrates that the scattering behaviour is dominated by the total surface area of the particles in the dispersion, when Q begins considerably to exceed the inverse of the size of the primary particles which here is ~ 10 nm.

In the lower range of Q, there is no evidence of any interference maximum as is observed in dispersions of discrete particles of comparable size and concentration. In contrast the scattered intensity continues to increase monotonically, albeit with a reduction in the power law slope, (the broken line shown in Figure 24

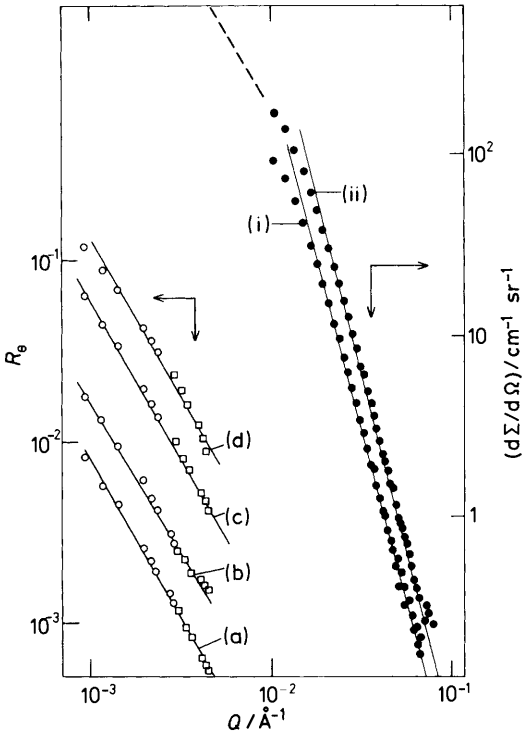

Figure 24 *Static light scattering and small angle neutron scattering of colloidal dispersions of silica particle aggregates of different concentrations. Concentrations for light scattering are: (a)* 3.4×10^{-4}, *(b)* 6.8×10^{-4}, *(c)* 1.7×10^{-3}, *and (d)* 3.4×10^{-3} g cm^{-3} *respectively; symbols* ○ *and* □, *correspond to measurements with* λ/nm *of* 546 *and* 365. *Concentrations (in* D_2O*) for SANS are:* (i) 0.10 *and* (ii) 0.23 g cm^{-3} *respectively; full lines correspond to slope of* ~ -3.9; *broken line to* -1.7

corresponds to an increase as $Q^{-1.7}$), until the lowest Q experimentally attainable ($Q_{min} \sim 1 \times 10^{-2}$ Å^{-1}) is reached.

Light scattering results obtained at lower Q are also shown in Figure 24 for several dispersion concentrations of the same aggregated silica. On account of multiple scattering and attenuation effects these measurements are restricted to considerably more dilute dispersions. Nevertheless it will be noted that the results all show a power law increase in $I(Q)$ with a power law exponent between -1.7 and -1.8, which is in accord with the limiting behaviour of $I(Q)$ at low Q observed in SANS. Such behaviour implies that the aggregates have fractal properties (*cf.* equation 34), and that these aggregates remain intact, and probably associate as the concentration of the dispersions is increased. Indeed there is evidence from SANS that the porous gels derived from these dispersions also retain fractal properties.

From similar studies made with other Aerosil silica dispersions[98] it has been shown that the fractal dimensionality falls within a range from ~ 1.6 to 2.0. This suggests that the aggregates have a relatively open structure, which is common to all the grades of Aerosil which have been studied. Furthermore, this value of D is similar to that of 1.75 which has been predicted by computer simulation for the process termed cluster aggregation (CA), in which clusters are formed by the homogeneous aggregation of a collection of particles; these small clusters subsequently diffuse and stick together to give larger aggregates.[108] It would seem possible that a comparable structure may arise here as a result of particle aggregation processes which occur during the vapour phase production of Aerosil powders. Although such a possibility will require further study, it is evident that the scattering behaviour is significantly different to that predicted for a structure formed by diffusion-limited aggregation, which involves the accretion of single diffusing particles onto a seed aggregate. The latter structure results in a D of ~ 2.5, which implies a much slower fall-off in the particle density correlation function, whereas cluster–cluster aggregation results in a highly ramified structure, as depicted in two dimensions in Figure 25. It is significant furthermore that electron microscopy of Aerosil powders shows particle aggregates containing chain-like formations.

The overall size of the aggregates is indicated by the lower Q value where a departure from power law behaviour occurs, as illustrated schematically in Figure 25. Thus a decrease in slope begins to occur in Figure 24 at $Q_1 \lesssim 10^{-3}$ corresponding to a size, a_1, of about 100 nm. This size corresponds to the range of self similarity, whereas the effective size of the aggregates will be somewhat larger due to a few particle chains extending beyond this range. From this it is evident that the average number of particles in an aggregate may exceed 10^3 (*cf.* equation 37).

6 Conclusion

In this review we have confined our attention to the determination of structure and interactions in oxide sols, giving particular emphasis to the application of light scattering and SANS techniques. As with other colloidal dispersions, it is apparent that a knowledge of these properties is important for an understanding of the factors which control the stability and rheology of these systems. However, the

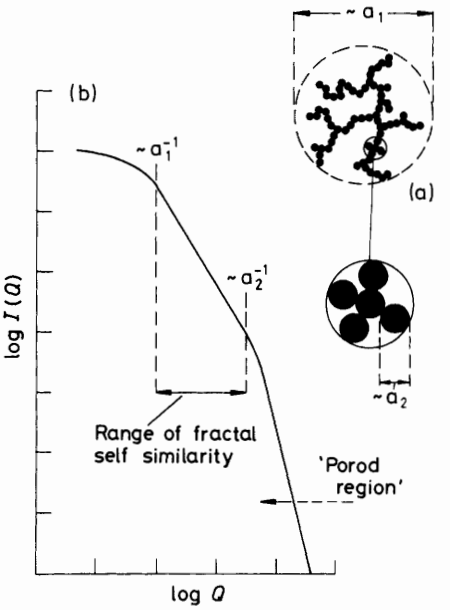

Figure 25 *Schematic representation of a particle aggregate (a) having a range of self similarity between approximately a_1 and a_2. The form of the scattering expected is as depicted in (b)*

recognition that the structure and interactions in relatively dilute sols may predetermine the microstructure of the porous gels which finally result on dehydration, makes these properties of overriding technological significance, as has recently been described.[37,60]

Although the application of SANS to the determination of structure and interactions in oxide sols has been described here, it is nevertheless evident that the SANS technique is highly versatile and applicable to a wide range of colloidal systems, as has already been extensively demonstrated. In the future, further rapid developments are to be expected as time-resolved scattering studies become possible. This may allow investigations of relaxation processes of colloidal particles under the influence of shear or when subjected to electric and magnetic fields for example. Such investigations of structure and interactions may be of particular interest with inorganic colloids such as oxide and clay sols which can exhibit complex rheological and thixotropic behaviour. Important progress in this direction has already been made in studies of surfactant micelles[112] and polymer solutions[113] under steady shear, where marked birefringence effects have been

[112] J. B. Hayter and J. Penfold, *J. Phys. Chem.*, 1984, **88**, 4589.
[113] R. C. Oberthür, in 'The Neutron and its Applications, 1982', ed. P. Schofield, Inst. Physics, Conf. Ser. No. 64, 1983, p. 321.

observed. Other important developments have been made in structural studies of ferromagnetic colloids, known as ferrofluids,[114] under the influence of magnetic fields. These SANS investigations have also exploited the phenomenon of the magnetic interaction of the neutron with atoms having unpaired electron spins. The kinetics and mechanism of flocculation processes is another potential area where time-resolved studies may make significant contributions to present understanding.

The contrast variation technique, which is a unique feature of SANS, has not been exploited extensively in studies of inorganic colloids as has been the case for biological systems for example. However, the possibilities have been recently impressively demonstrated by structural studies of surfactant- and polymer-stabilized calcium carbonate dispersions in liquid hydrocarbons.[115] Most SANS studies of colloids hitherto have been restricted to ambient conditions, although their behaviour far removed from these may be of interest. Because there are few restrictions on the sample environment in neutron scattering, *in situ* studies of colloids under these conditions are feasible, as has recently been demonstrated by the investigation of silica sols in water at high temperatures and pressures.[116]

Work described in this review was undertaken as part of the Underlying Research Programme of the UKAEA.

[114] R. Pynn, J. B. Hayter, S. W. Charles, *Phys. Rev. Lett.*, 1983, **51**, 710.
[115] I. Markovic, R. H. Ottewill, D. J. Cebula, I. Field, and J. F. Marsh, *Colloid Polym. Sci.*, 1984, **262**, 648.
[116] J. Bunce, J. D. F. Ramsay, and J. Penfold, *J. Chem. Soc., Faraday Trans. 1*, 1985, **81**, 2845.